Doping of TiO₂ Using Metal Waste (Door Key) to Improve Its Photocatalytic Efficiency in the Mineralization of an Emerging Contaminant in an Aqueous Environment

Dany Edgar Juárez-Cortazar [1], José Gilberto Torres-Torres [1], Aracely Hernandez-Ramirez [2], Juan Carlos Arévalo-Pérez [1], Adrián Cervantes-Uribe [1], Srinivas Godavarthi [1], Alejandra Elvira Espinosa de los Monteros [1], Adib Abiu Silahua-Pavón [1] and Adrián Cordero-Garcia [1,*]

[1] Laboratory of Catalytic Nanomaterials Applied to the Development of Energy Sources and Environmental Remediation, Tabasco Applied Science and Technology Research Center (CICTAT), Universidad Juárez Autónoma de Tabasco, DACB, Km.1 Carretera Cunduacán-Jalpa de Méndez, Cunduacán 86690, Tabasco, Mexico; internacional_celeste@hotmail.com (D.E.J.-C.); gilberto.torres@ujat.mx (J.G.T.-T.); carlos.arevalo@ujat.mx (J.C.A.-P.); adrian.cervantes@ujat.mx (A.C.-U.); srinivas.godavarthi@gmail.com (S.G.); ale2962@gmail.com (A.E.E.d.l.M.); adibab45@gmail.com (A.A.S.-P.)

[2] Facultad de Ciencias Químicas, UANL, Universidad Autónoma de Nuevo León, Ciudad Universitaria, San Nicolás de los Garza 66451, Nuevo León, Mexico; aracely.hernandezrm@uanl.edu.mx

* Correspondence: adrian.cordero@ujat.mx; Tel.: +52-993-591-0296

Abstract: Photocatalysis is an effective advanced oxidation process to mineralize recalcitrant contaminants in aqueous media. TiO₂ is the most used photocatalyst in this type of process. To improve the deficiencies of this material, one of the most used strategies has been to dope TiO₂ with metallic ions. Chemical reagents are often used as dopant precursors. However, due to the depletion of natural resources, in this work it was proposed to substitute chemical reagents and instead use a metallic residue (door key) as a doping precursor. The materials were synthesized using the sol–gel method and calcined at 400 °C to obtain the crystal structure of anatase. The characterization of the materials was carried out using X-ray diffraction (XRD), transmission electron microscopy (TEM), diffuse reflectance spectroscopy (DRS), scanning electron microscopy–energy-dispersive X-ray analysis (SEM-EDX) methods X-ray photoelectron spectroscopy (XPS), and inductively coupled plasma optical emission spectroscopy (ICP-OES). The results obtained indicate that Cu⁺/Cu²⁺ and Zn²⁺ ions coexist in the support, which modifies the physicochemical properties of TiO₂ and improves its photocatalytic efficiency. The synergistic effect of the dopants in TiO₂ allowed the mineralization of diclofenac in an aqueous medium when T-DK (1.0) was used as photocatalyst and simulated solar radiation as an activation source.

Keywords: emerging contaminant; photocatalysis; TiO₂ doped; discarded metal waste; sol–gel

1. Introduction

Heterogeneous photocatalysis is an advanced oxidation process that has proven to be effective for the mineralization of recalcitrant contaminants in an aqueous medium. The most efficient photocatalyst for the photocatalytic process is TiO₂ since it has optical, structural, and organoleptic properties, making it efficient in the mineralization of contaminants in an aqueous medium. However, this semiconductor has the disadvantage of having an Eg 3.2 eV, which means that it cannot be activated with UV light, so it absorbs only 5% of solar radiation [1–3]. This restricts the use of solar radiation as an activation source.

Various strategies have been developed to improve the spectral response in the visible region of photocatalytic oxides. One of the most widely used strategies has been to alter the physicochemical properties of oxide by incorporating metallic ions into its crystalline structure [4,5]. It has been shown that metal doping of TiO₂ causes the formation of

new energy levels below the conduction band and delays the rapid recombination of electron–hole pairs, which increases the photocatalytic activity of this semiconductor [6,7].

To synthesize TiO_2 doped materials, transition metal salts are used. However, based on analysis by the World Metal Reserve, production from a mine has a shorter timescale than mineral deposit formation, suggesting that known primary metal supplies will be depleted. Importantly, the risk of contamination by heavy metals is higher since they are not chemically or biologically degradable. Once disposed of, they can remain in the environment for hundreds of years and cause environmental damage. It has been shown that the discharged metals are easily transported through groundwater, causing contamination of soil and rivers [8], as well as the degradation and death of vegetation, animals, and even direct damage to humans [9,10]. Therefore, in our research group, we are convinced that the recycling of metals that we use in our daily lives helps conserve the natural riches of the environment and favors the reduction of environmental pollution. Among metal scrap, door keys are among the most common forms of consumer waste. The door key used as a doping precursor was taken from a metal scrap yard; hence, it had advanced metal wear. Due to this, its origin of manufacture is unknown. However, it is known that most door keys are alloys of steel or brass.

Among the metals that compose these alloys, nickel, copper, and zinc are chemical elements widely used to dope TiO_2 nanoparticles [11–13]. Such is the case of a study carried out by Raguram, T. et al. [11], who synthesized TiO_2-Ni nanoparticles using the sol–gel method. The results reported by the researchers indicate that the doping of Ni^{2+} in TiO_2 benefited the absorption of visible light, reaching a maximum of 61.04% in the degradation of the methylene blue dye in an aqueous medium. On the other hand, Hemraj, Y. et al. [12] synthesized TiO_2 nanoparticles doped with different Cu^{2+} contents (0 to 3.0% mol) using the sol–gel method for semiconductor synthesis. The results show that the TiO_2-Cu nanoparticle (3.0%) has a photocatalytic efficiency superior to pure TiO_2. They mentioned that the improvement in the photocatalytic performance for the photodegradation of methyl orange was due to the redshift of the bandgap energy (Eg) and the decrease in the recombination rate of the electron–hole pair of TiO_2-Cu nanoparticles. In general, it has been mentioned that noble metals such as Ni and Cu are good candidates to act as traps for photogenerated electrons because the Fermi level of these ions is lower than that of TiO_2. Regarding Zn use in TiO_2 doping, Shao, M. et al. [13] concluded that adding Zn to TiO_2 reduces Eg and increases optical absorption in the visible region, reaching a maximum rate of 88.14% in degradation of tetracycline. In addition to the above, many researchers have focused on multi-doping metals (bimetallic or trimetallic) over the last few years. They mention that the second metal can alter the electronic properties and the formation of active surface structures, increasing the photocatalytic activity of TiO_2 concerning monometallic doping [14–17]. The previous work provides evidence of the feasibility of using transition metals as monometallic or bimetallic dopants in TiO_2 nanoparticles using chemical reagents as doping precursors. However, we did not find any scientific report investigating the use of door-key waste for TiO_2 multidoping. As an additional motivation, it is important to mention that innovative strategies are currently being developed to increase the efficiency of contaminant removal and transformation [18–22]. In this context, an innovative synthesis route was designed to obtain TiO_2 doped with metallic ions, where the use of chemical reagents is avoided, and it was proposed to use a metallic residue (door key) as a doping precursor to improving the photocatalytic efficiency of TiO_2 in the mineralization of an emerging contaminant.

2. Materials and Methods

2.1. Chemicals and Reagents

To synthesize TiO_2, reagent grade chemicals were used without further purification. Titanium (IV) butoxide (97%), 1-butanol anhydrous (99.8%), and nitric acid ($\geq$65%) were purchased from Sigma-Aldrich. Deionized water was used for the hydrolysis step during

the sol–gel synthesis process. A door key recovered from a metal scrapyard was used as a doping precursor.

2.2. Synthesis of Photocatalysts

To analyze the effect of metal ions that make up the door key on the photocatalytic activity of TiO_2, 3 samples were prepared with different percentages of metallic waste (0, 0.5, and 1.0 wt.%). The materials nomenclature is defined as T, T-DK (0.5), and T-DL (1.0) as well as the abbreviation T (TiO_2) + the metal residue percentage number (DK).

The synthesis of the photocatalysts was carried out using a non-traditional sol–gel synthesis route. The waste door key (0.5 or 1.0 wt.%) for the TiO_2 doping was dissolved at room temperature in 1.5 mL of HNO_3. *Solution A*. To synthesize TiO_2, doped titanium (IV) butoxide and anhydrous 1-butanol were mixed. *Solution B*. After stirring for 30 min at room temperature, *solution A* was added drop by drop to *solution B*, continuing to stir for 30 min. To begin the hydrolysis reaction in the *A–B* mixture, 10 mL of deionized H_2O was added per drop. The gel obtained was aged at ambient temperature for 24 h. Xerogel was subsequently obtained by filtering the gel with a vacuum pump to remove the solvents and then drying for 12 h at 60 °C. Finally, the xerogel was heat-treated at 400 °C for 4 h using a $4 °C\ min^{-1}$ heating ramp with a static air atmosphere. Pure TiO_2 was synthesized using a similar methodology as described earlier for comparison purposes. The only difference is that for pure TiO_2 synthesis, *solution A* had no metallic ions.

2.3. Characterization of Photocatalysts

The surface area of the photocatalysts was determined using the BET method. Their N_2 adsorption–desorption isotherms were obtained at -196 °C using Asap 2020 equipment after degassing samples at 250 °C for 12 h in a high vacuum.

The crystalline phase for each sample was determined using a Siemens D500 X-ray diffractometer (XRD) with Cu K_α radiation ($\lambda = 0.15418$ nm). The diffraction patterns were obtained within the range of 10 to 80° at an acquisition rate of $0.02\ s^{-1}$ and 1 s per point. The average crystal size was calculated using the Scherrer equation.

$$\Phi = \frac{K\lambda}{\beta \cos \theta} \tag{1}$$

where Φ is the size of the crystal, K (0.91) is the form factor, λ is the wavelength of the X-rays, β is the width at half height (FWHM) of the main intensity peak, and θ is the Bragg angle.

The optical properties of the materials were obtained with diffuse reflection spectroscopy (DRS) using a Perkin-Elmer UV-Vis spectrophotometer with an integrating sphere. Absorption spectra were recorded in the range from 300 to 800 nm. A barium sulfate plate ($BaSO_4$) was used as a reference. Based on the absorption spectra, the bandgap energies of the photocatalysts were determined using the Kubelka–Munk theory and Tauc plot [23].

The morphological characterization of composites was conducted with transmission electron microscopy (HRTEM) using a JEOEL electronic microscope model JEM2100.

The semi-quantitative elementary composition of the materials was determined with energy-dispersive X-ray spectroscopy (EDX) using an electron scanning microscope with Rontec Xflash detector model Hitachi S-4700 Type IIc. In addition, the chemical composition of the catalysts was determined using inductively coupled plasma optical emission spectroscopy (ICP-OES) Varian 725-ES, after acidic digestion (Nitric Acid) of the materials.

The XPS spectra were obtained using X-ray photoelectron spectroscopy (XPS) with Thermo Scientific apparatus equipped with a non-monochromated Mg anode as an X-ray source operated at 12 kV under vacuum (2×10^{-7} mbar). The binding energies were calibrated at 284.6 eV with respect to the C1s peak of the carbon samples. The XPS spectrums were deconvoluted using the PeakFit software. The peaks were fitted to a linear background and a combination of Gaussian/Lorentzian functions.

2.4. Evaluation of Photocatalytic Activity

Diclofenac was used as a contaminant to evaluate the photocatalytic activity of photocatalysts. The photocatalytic degradation of 10 ppm of diclofenac (Sigma-Aldrich, Burlington, MA, USA, ≥98.5%) was carried out in a glass reactor with a volume of 0.5 L and photocatalyst load of 1.0 gL^{-1}. The reactor was placed in a SUNTEST XLS+ solar simulator, equipped with a xenon arc lamp model XL-S-750 and a 320 nm cut-off filter. During the experiments, the temperature of the reaction system was maintained in the range of 25 to 35 °C. The suspension was stirred in the dark for 30 min while the air was bubbled into the system. The light was then turned on, and simultaneously the system continued to be supplied with air. To monitor the mineralization of diclofenac, samples were collected from the reactor every 30 min to up 180 min. Photolysis experiments were also carried out for comparative purposes. The progression of the mineralization of the contaminant was followed by the measurement of total organic carbon using a Shimadzu TOC-VSCH analyzer. The following equation determined the mineralization of diclofenac:

$$\%TOC = \frac{TOC_0 - TOC_f}{TOC_0} \times 100 \qquad (2)$$

where TOC_0 is the mineralization at time zero and TOC_f is the final mineralization at each instant.

3. Results

3.1. Sample Characterization

3.1.1. XRD

The XRD patterns for pure and doped samples are illustrated in Figure 1. In all diffractograms, peaks are observed at angles 25.33, 37.8, 48.06, 53.9, and 55.08, characteristic of TiO_2-anatase (JCPDS card no. 21-1272). The crystalline phase obtained corresponds to that reported by other investigators. Other studies mention that the crystalline phase of anatase occurs when heat treatment varies between 200 and 500 °C. It was said that the amount and physicochemical properties (high ionic radii and electronic status) of the doping metal can influence the rate of transformation of anatase to the rutile phase [24,25]. Such is the case of a study conducted by Hampel et al. [25]; they observed that TiO_2 doped with 5 wt.% Cu ions, calcined at 450 °C, contained an anatase phase and a rutile phase fraction, which increased with increasing Cu concentration from 5 to 10 wt.%. In our case, the dopant concentration does not influence the anatase–rutile transition because the maximum theoretical concentration of doping ions in TiO_2 is less than 1 wt.%.
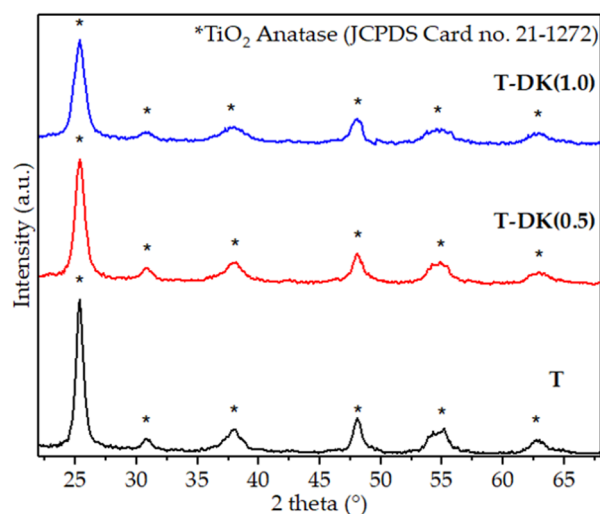

Figure 1. X-ray diffraction (XRD) patterns of TiO_2 and doped-TiO_2.

It is convenient to have TiO$_2$ nanoparticles with an anatase crystalline structure for this research. There is evidence that other polymorphic forms of this material are less effective in photocatalytic reactions. This is due to the higher adsorption capability of O$_2$ on the surface of the anatase phase than in the rutile phase. The adsorbed oxygen is reduced to superoxide radicals (O$_2^{\bullet-}$) by photoexciting electrons from BV to BC, thus functioning as an electron trap, inhibiting the recombination of e$^-$/h$^+$ pairs. This increases the half-life of the redox reactions that benefit the formation of hydroxyl radicals (OH$^\bullet$) with sufficient oxidation potential for the photocatalytic degradation of recalcitrant compounds. Along with the above, the redox potential of BV in anatase is more negative, making it more competitive than the rutile phase for oxidation reactions [26–28].

No characteristic peaks were associated with doping Cu, Zn, or Ni (metal oxide). It is known that X-ray diffractometers are not sensitive to levels of impurities lower than 5%. For this reason, the absence of characteristic peaks of the dopant ions can be attributed to the fact that the percentages of door lock used during the synthesis of the doped TiO$_2$ were less than 1 wt.%. Likewise, this also suggests that the doping ions could be highly dispersed in the titania support.

For doped TiO$_2$ nanoparticles, the maximum intensity of the anatase phase crystalline plane (101) decreases. This indicates that the crystallization of TiO$_2$ anatase is restricted due to the increase in the content of the dopant (0.5 to 1.0 wt.%). As shown in Table 1, the increase in the doping content leads to an average particle size smaller than the pure material. The decrease in crystalline nature has been reported by other authors who used Cu and Zn salts as doping precursors. They mentioned that a mechanism of fixation of doping ions at the grain boundary inhibits anatase nanoparticle growth [29–31].

Table 1. Material characterization results of TiO$_2$ and doped-TiO$_2$.

Catalyst	Cu wt.%			Zn wt.%			Average Particle Size (nm)		Eg (eV)
	Sol. A [1]	EDX	ICP-OES	Sol. A [1]	EDX	ICP-OES	DRX	SEM	
T	nd	nd	nd	nd	nd	nd	19.50	21	3.23
T-DK (0.5)	0.21 ±0.009	0.19 ±0.002	0.23 ±0.014	0.13 ±0.005	0.12 ±0.004	0.11 ±0.003	15.7	16	2.90
T-DK (1.0)	0.47 ±0.011	0.43 ±0.015	0.44 ±0.009	0.24 ±0.008	0.22 ±0.007	0.21 ±0.006	11.3	11	2.76

[1] Sol. A: Solution resulting from the digestion of the dopant precursor.

3.1.2. HRTEM and Elemental Analysis

In the HRTEM micrographs in Figure 2, pure and doped TiO$_2$ nanoparticles exhibit spherical morphology. After doping, it is also observed that the average crystal size decreases compared to pure TiO$_2$. This phenomenon has already been explained in the XRD diffractogram discussion. Based on the histograms in Figure 2, for T and T-DK (1.0), the average particle size was similar to those obtained with XRD.

Although it has been shown that the surface area is not decisive in the photocatalytic process, as a result of particle size decrease, the specific surface area increased gradually from 58.8 ± 0.8 m^{2}g^{-1} for T, 76 ± 0.4 m^{2}g^{-1} for T-DK (0.5), and 88.7 ± 0.5 m^{2}g^{-1} for T-DK (1.0). Increased dopants in TiO$_2$ inhibit particle growth; consequently, the narrow pore size distribution and the surface becomes larger [32].

From the HRTEM micrography in Figure 2, it is difficult to determine the presence of doping ions. Nevertheless, the elementary EDS and ICP-OES analysis results, summarized in Table 1, show that doped TiO$_2$ nanoparticles contain Cu and Zn doping ions. According to the EDS images in Figure 2, these dopants are homogeneously distributed over the surface of the TiO$_2$. The presence of Ni ions was not detected. As the dopant precursor was obtained from a junkyard, it had advanced metal wear, so there was no longer any nickel coating that this type of door key usually has. So, the absence of nickel in the elemental

analysis performed by EDS and ICP-OES was an expected result. This means that only copper and zinc were considered doping ions.
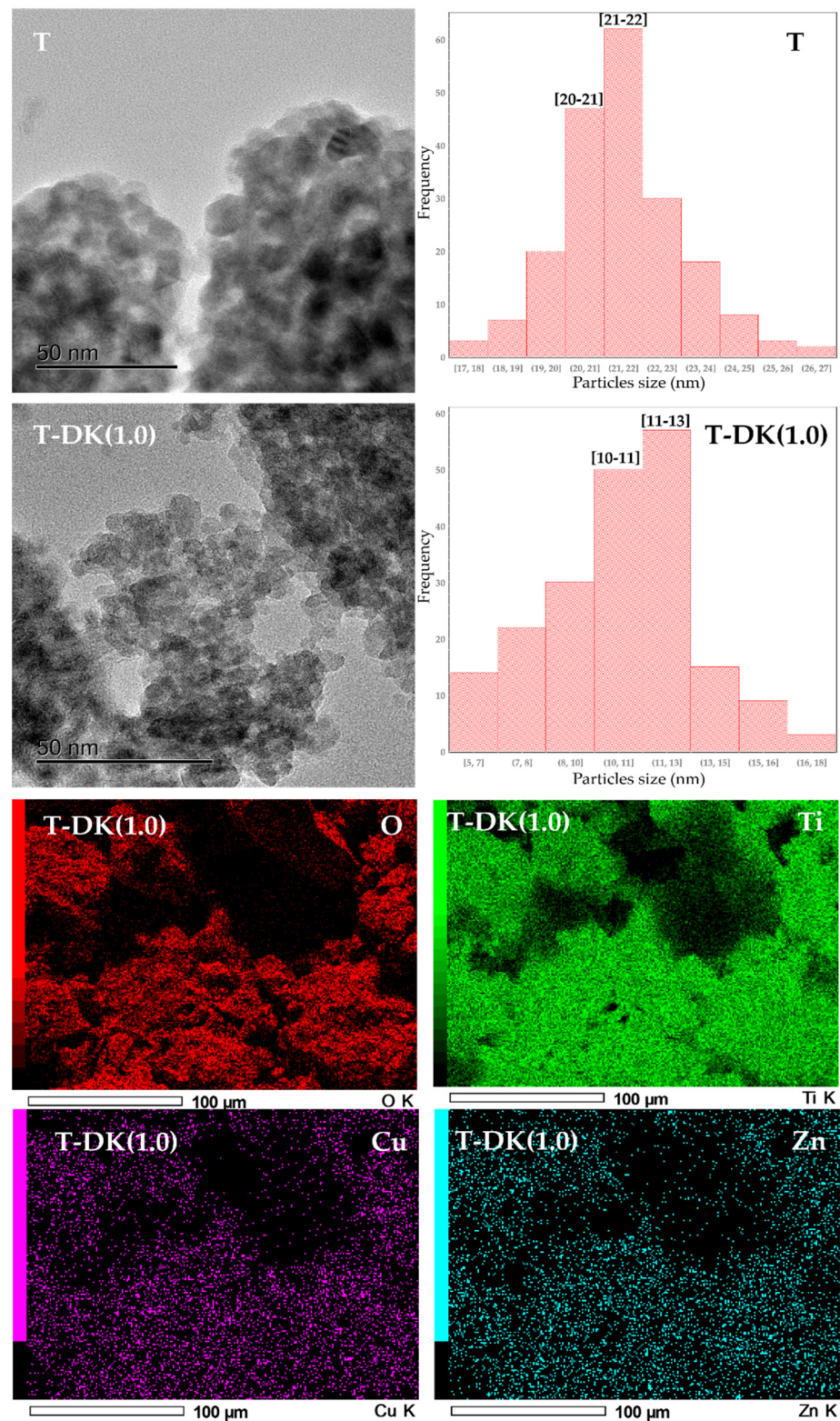

Figure 2. HRTEM micrographs, histograms, and EDS spectra of TiO_2 pure and T-DK (1.0).

Regarding the weight percentage of Cu and Zn in TiO_2, EDS and ICP-OES (Table 1) show differences between the theoretical weight percentage of Cu and Zn concerning the real percentage. To explain this difference, elemental analysis by ICP-OES was performed

on solution A (solution resulting from the digestion of the metal residue). The results show that during the digestion carried out in an open system, part of the initial concentration of the doping ions is lost (Table 1). The efficacy of the digestion method, among other variables, will be investigated in future projects.

3.1.3. DRS

The optical properties of these materials were obtained using DRS. The absorption spectra are shown in Figure 3. Bandgap values (Eg) are shown in Table 1. Pure TiO_2 exhibits strong absorption at 396 nm (3.23 eV), assigned to the charge transfer of the metal-ligand in Ti^{4+}(3d)-O^{2-}(2p). For T-DK (0.5) and T-DK (1.0), the door key used as a dopant influenced the optical properties of TiO_2 since the optical absorption band decreased below 396 nm with the increase in the percentage by weight of dopant ions. The T-DK (0.5) material presented a bandgap of 2.90 eV, and the T-DK (1.0) material showed a bandgap of 2.76 eV. It is known that the value of the bandgap of ZnO (Eg ≈ 3.2 eV) is similar to that of TiO_2 (Eg ≈ 3.23 eV) [33], so zinc does not promote the decrease in Eg. The decrease is due to a redistribution of the electric charge of TiO_2 caused by copper ions in interstitial positions or to copper oxides (Eg ≈ 2.5 eV) formed [34]. The obtained Eg values indicate that in our materials, the valence electrons can be transferred to the conduction band using lower energy (visible light) than that required to activate pure TiO_2 (UV light).
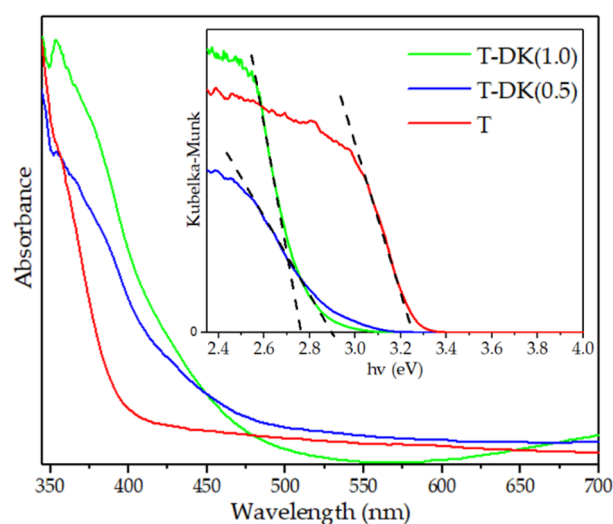
Figure 3. Absorption spectrum of T, T-DK (0.5), and T-DK (1.0). Insets: bandgap energy values: linear part of the plot extrapolated to the X-axis.

For T-DK (1.0), the absorption band at 600 nm suggests a $^2B_{1g}{\rightarrow}^2B_{2g}$ characteristic of octahedral coordination with tetragonal distortion around Cu^{2+} [34,35]. For low concentrations of copper, T-DK (0.5), no characteristic bands corresponding to metallic ion species were observed. Likewise, no interfacial charge transfer bands were observed from the valence band of TiO_2 to the valence band of zinc oxides. This is probably due to the low weight concentration of the dopant ions or their good dispersion on the titania surface.

3.1.4. X-ray Photoelectron Spectroscopy

The XPS spectra of T and T-DK (1.0) were obtained to determine the oxidation state of the material components. The oxidation states in the O 1s, Cu2p, and Zn 2p regions were obtained by deconvoluting their peaks. The PeakFit software version 4.1.2, AISN Software Inc, was used to this effect. The correlation coefficients (r^2) of the deconvoluted peaks were higher than 0.99. The spectrum in Figure 4a shows bands at 458.5 and 464.1 eV, characteristic of the binding energy of Ti $2p_{3/2}$ and Ti $2p_{1/2}$ in TiO_2 [36]. The observed band comprises two peaks in the O1s region of pure TiO_2. One of these, located at 530.02 eV, is assigned to ionic oxygen in the crystalline array (O-Ti^{4+}). The small peak at 531.82 eV is

related to adsorbed OH groups, chemisorbed O species, or oxygen vacancies [37]. These same bands were observed in the Ti 2p (Figure 4c) and O 1s (Figure 4d) regions of the XPS spectra obtained for T-DK (1.0). However, a shift in the binding energies of the Ti 2p and O 1s bands is observed for this material. It is known that the binding energy depends on the oxidation state and the local chemical environment of titanium and oxygen [38,39]. Since the electronegativity of Cu (1.9) and Zn (1.65) is greater than that of Ti (1.54), the electron density around the oxygen ions decreases, which causes an increase in the binding energy.
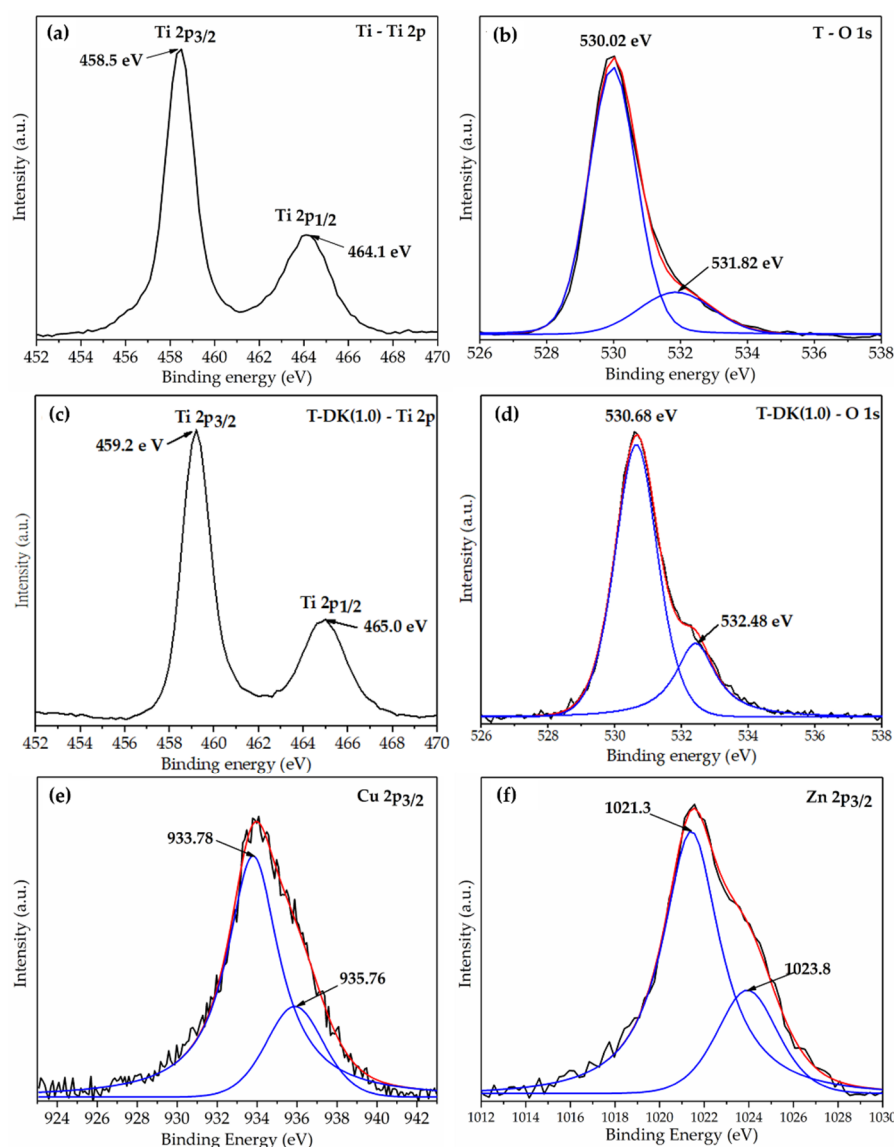

Figure 4. XPS spectra of TiO_2 and T-DK (1.0): (**a**,**b**) Ti 2p, (**c**,**d**) O 1s, (**e**) Cu 4d, and (**f**) Zn 4d.

To develop the above, the Cu 2p (Figure 4e) and Zn 2p (Figure 4f) XPS spectra from the T-DL (1.0) photocatalyst were analyzed. In Figure 4e, the binding energies at ~933.78 eV correspond to Cu^+ from Cu_2O, while the binding energies ~935.76 eV can be assigned to Cu^{2+} in the form of CuO or $Cu(OH)_2$ [25,39,40]. In the case of zinc ions, a typical peak of Zn $2p_{3/2}$ is observed in Figure 4f. The deconvolution of this peak produced two peaks at 1021.3 and 1023.8 eV. The strongest peak located at 1021.3 eV is associated with Zn^{2+} ions in the ZnO with an arrangement of wurtzite crystal. Peak at 1023.8 eV belongs to Zn^{2+} ions in $Zn(OH)_2$ [41–43].

The ionic radius of Ti^{4+}, Cu^{2+}/Cu^+, and Zn^{2+} is 0.061, 0.73/0.77, and 0.74 Å, respectively [44]. These data indicate a significant difference between the values of the ionic radii

of the dopants with titanium. As a result, the substitution process of Ti ions by Cu^{2+}/Cu^{+} and Zn^{2+} is limited by the difference between their ionic radii. According to the principles of Hume-Rothery [45], lattice substitution between atoms can only happen if the difference between them is less than 20%. Theoretical studies for copper ions argue that, for the substitution of titanium ions in the crystalline structure, the maximum concentration of copper should be 0.3% [39]. As a result, we can report that some copper and zinc ions were aggregated as oxides on the surface of TiO_2 nanoparticles, creating a heterojunction between these semiconductor materials. Other doping ions held interstitial positions within the crystalline network of the TiO_2 anatase.

According to the results of the material characterization and the references used for their discussion, the interaction between the support and the copper and zinc ions is similar to that reported by other investigations in which the dopant precursor is a chemical reagent.

3.2. Photocatalytic Activity Measurement

To evaluate the photocatalytic activity of the synthesized materials, a solution of diclofenac at a concentration of 10 ppm was used. Total organic carbon (TOC) values are summarized in Table 2. All the materials showed photocatalytic activity in the degradation of diclofenac (Figure 5a,b). Nevertheless, for doped materials, the increased content of doping ions enhanced the photocatalytic activity of TiO_2. The best activity was achieved when T-DK (1.0) was used as a photocatalyst, obtaining up to 94% of mineralized diclofenac. The values for the rate constants (Table 2 and Figure 5b) are consistent with what is seen in Figure 5a. This means that with T-DK (1.0), the maximum mineralization is achieved, but this transformation is also carried out in less time than with T and T-DK (0.5).
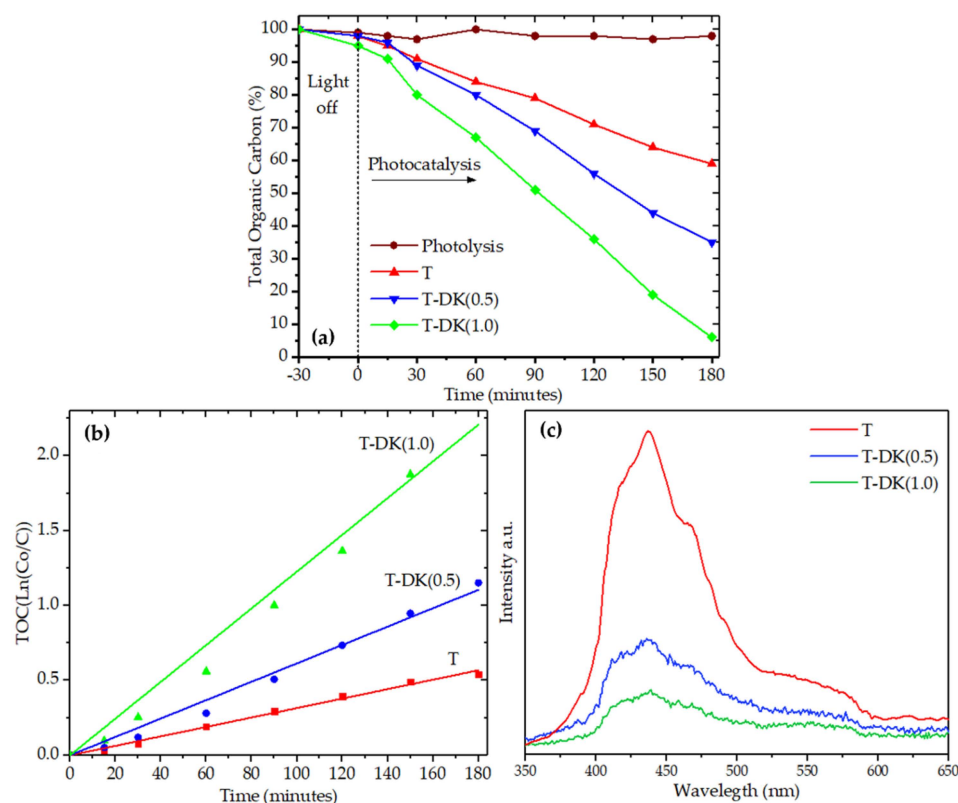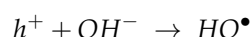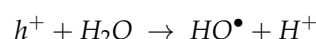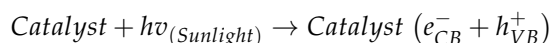

Figure 5. (**a**) Total organic carbon, (**b**) kinetic constants, (**c**) PL spectra of undoped and codoped TiO_2.

Table 2. Apparent first-order rate constants obtained for the diclofenac mineralization.

Catalyst	Residual TOC (%)	K_{app} (min^{-1})	$t_{1/2}$ (min)	R^2
T	59	3.2×10^{-3}	216.61	0.997
T-DK (0.5)	35	6.1×10^{-3}	113.63	0.993
T-DK (1.0)	6	1.23×10^{-2}	56.35	0.990

The correlation of material characterization results with photocatalytic test results suggests that the increase in photocatalytic activity is due to two factors:
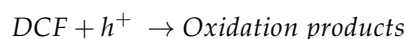
i. First, the doping ions induced the reduction of Eg in TiO$_2$ (see Table 1). The decrease in the value of Eg for T-DK (0.5) and T-DK (1.0) indicates that these materials can be activated with visible light radiation. This means solar light absorption is more efficient in doped TiO$_2$ than pure TiO$_2$ [46]. This increases the efficiency of generating electron–hole pairs that initiate redox reactions that directly or indirectly produce the hydroxyl radicals that cause the pollutant to be mineralized. Due to the many possible reaction mechanisms during the diclofenac mineralization process, those considered the main ones in the photocatalytic mechanism are given below [24].

$$Catalyst + hv_{(Sunlight)} \rightarrow Catalyst \left(e_{CB}^- + h_{VB}^+ \right)$$

$$h^+ + H_2O \rightarrow HO^\bullet + H^+$$

$$h^+ + OH^- \rightarrow HO^\bullet$$

Hydroxyl radical attack:

$$DCF + HO^\bullet \rightarrow Degradation\ products$$

Oxidation by the positive hole:

$$DCF + h^+ \rightarrow Oxidation\ products$$

ii. Second, the synergistic effect of the dopant species inhibited the recombination of the e$^-$/h$^+$ pairs. This information was obtained by analyzing the charge carrier recombination of each synthesized material. In the emission spectra in Figure 5c, pure TiO$_2$ obtained the higher intensity emission spectra, meaning rapid recombination of the electron–hole pairs. Contrary to TiO$_2$, the intensity of the emission spectra was lower when the percentage by weight of the doping ions increased, which suggests a low recombination rate for the electron–hole pairs photogenerated in T-DK (0.5) and T-DK (1.0). According to the results obtained using XPS, in doped TiO$_2$ Cu^{2+} and Zn^{2+} ions in interstitial positions and oxides of the doping ions coexist. The low recombination of photogenerated charge carriers at T-DK (0.5) and T-DK (1.0) can be understood due to the positions of the band edges of the oxides in the heterojunction. The measured conduction band (CB) potential values of TiO$_2$ and CuO are –0.35 and +0.12 V (vs. SCE), respectively. The valence band of TiO$_2$ is lower than ZnO by about 0.36 V (vs. NHE), and this is superior to CuO by approximately 0.20 V (vs. SHE). The relative position difference of the energy band of CuO and ZnO charge transfer occurs between them and TiO$_2$. Thus, an electron photogenerated in TiO$_2$ is transferred from the conduction band of this semiconductor to ZnO and CuO, acting as an electron trap to inhibit their recombination. Concurrent with the above, hole transfer can arise from the valence band (VB) of TiO$_2$ to the VB of ZnO and CuO [43,44,47,48]. Therefore, in addition to the decrease in Eg, the coupled effect between energy bands of TiO$_2$, CuO, and ZnO was an essential factor to suppress the recombination of the electron–hole pairs, improving the photocatalytic activity of doped TiO$_2$.

An important characteristic of photocatalysts is their chemical stability after several recycling cycles. Therefore, the reuse of T-DK (1.0) was evaluated during five consecutive reuse cycles. The percentage results in Figure 6a show that during the five cycles of reuse, the mineralization efficiency of diclofenac was in the range of 92.5 to 95%, with a standard deviation of ±1.48. Consequently, no significant change in the mineralization efficiency of diclofenac was observed. The stability in the photocatalytic activity is because the concentration of the dopant ions (Figure 6a) and the crystal structure of the TiO_2-anatase (Figure 6b) does not change before or after the reuse cycles. A similar effect occurs for the photocatalyst morphology determined by SEM in Figure 6c,d. This means that the photocatalyst T-DK (1.0) has a high activity and stability during the five cycles of diclofenac photocatalytic mineralization.
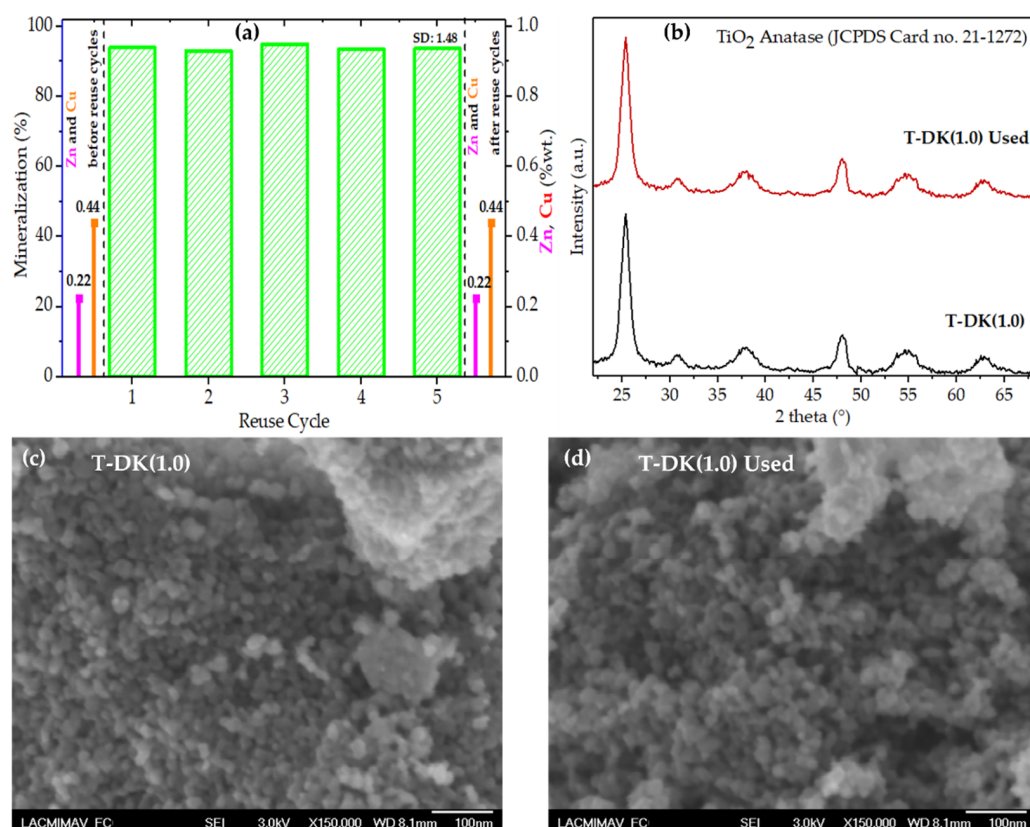

Figure 6. Reuse cycles using T-DK (1.0) and elemental analysis of Cu and Zn before and after the reuse cycle (**a**). DRX diffractograms (**b**) and SEM micrographs of T-DK (1.0) before and after five cycles of reuse (**c**,**d**).

4. Conclusions

This work shows that incorporating Cu and Zn ions into TiO_2 is possible when a door key is used as a doping precursor. Material characterization showed that these ions were integrated into the support as Cu^+/Cu^{2+} and Zn^{2+}, occupying interstitial positions or forming heterojunctions between copper and zinc oxides with titania. The modification with both ions had a dual effect dependent on the concentration of the doping metals. First, an inverse correlation was observed between the concentration of doping ions and the Eg. This resulted in greater light absorption within the visible range. Second, it was shown that the impurities in TiO_2 acted as an electron trap, so the recombination of the e^-/h^+ pairs was lower for T-DK (1.0) than for TiO_2. Therefore, the photocatalytic activity of the synthesized materials occurred in the following order: T < T-DK (0.5) < T-DK (1.0).

The results obtained in this work confirm previous state-of-the-art findings: Doping TiO_2 with Cu and Zn ions or other metal ions is an efficient strategy to improve the photo-

catalytic activity of titania. As an additional contribution, it is possible to use discarded door keys as a doping precursor to improving the photocatalytic activity of TiO_2. Finally, these results open the door for future research. Other variables can be considered: method of digestion of the metal residue, method of synthesis of materials, pH of synthesis, and calcination temperatures, among other variables. These variables were not considered in this first study, as the main objective was to investigate the feasibility of using door keys as doping precursors.

Author Contributions: Conceptualization, Visualization, Formal analysis, Investigation, Validation, Writing—original draft, Writing—review and editing, D.E.J.-C.; Writing—original draft, Writing—review and editing, Resources, J.G.T.-T.; Writing—original draft, Writing—review and editing, Resources, A.H.-R.; Writing—original draft, Writing—review and editing, J.C.A.-P.; Writing—original draft, Writing—review and editing, A.C.-U.; Writing—original draft, Writing—review and editing, A.E.E.d.l.M.; Writing—original draft, Writing—review and editing, S.G.; Writing—original draft, Writing—review and editing, A.A.S.-P.; Conceptualization, Formal analysis, Funding acquisition, Investigation, Methodology, Project administration, Resources, Supervision, Validation, Visualization, Writing—original draft, Writing—review and editing, A.C.-G. All authors have read and agreed to the published version of the manuscript.

Institutional Review Board Statement: Not applicable.

Informed Consent Statement: Not applicable.

Data Availability Statement: Data are contained within the article.

Conflicts of Interest: The authors declare no conflict of interest.

References

1. Chen, D.; Cheng, Y.; Zhou, N.; Chen, P.; Wang, Y.; Li, K.; Huo, S.; Cheng, P.; Peng, P.; Zhang, R.; et al. Photocatalytic degradation of organic pollutants using TiO_2-based photocatalysts: A review. *J. Clean. Prod.* **2020**, *268*, 121725. [CrossRef]
2. Zambrano, J.; Irusta-Mata, R.; Jiménez, J.J.; Bolado, S.; García-Encina, P.A. Chapter 24—Photocatalytic removal of emerging contaminants in water and wastewater treatments: A review. *Dev. Wastewater Treat. Res. Processes* **2022**, *1*, 543–572. [CrossRef]
3. Naciri, Y.; Hsini, A.; Bouziani, A.; Djellabi, R.; Ajmal, Z.; Laabd, M.; Navío, J.A.; Mills, A.; Bianchi, C.L.; Li, H.; et al. Photocatalytic oxidation of pollutants in gas-phase via Ag_3PO_4-based semiconductor photocatalysts: Recent progress, new trends, and future perspectives. *Crit. Rev. Environ. Sci. Technol.* **2021**, *52*, 1–44. [CrossRef]
4. Tanji, K.; Zouheir, M.; Naciri, Y.; Ahmoum, H.; Hsini, A.; Mertah, O.; El Gaidoumi, A.; Navio, J.A.; Hidalgo, M.C.; Kherbeche, A. Visible light photodegradation of blue basic 41 using cobalt doped ZnO: Box–Behnken optimization and DFT calculation. *J. Iran. Chem. Soc.* **2022**, *18*, 1–16. [CrossRef]
5. Tanji, K.; Zouheir, M.; Hachhach, M.; Ahmoum, H.; Jellal, I.; El Masaoudi, H.; Naciri, Y.; Huynh, T.-P.; Nouneh, K.; Benaissa, M.; et al. Design and simulation of a photocatalysis reactor for rhodamine B degradation using cobalt-doped ZnO film. *React. Kinet. Mech. Catal.* **2021**, *134*, 1017–1038. [CrossRef]
6. Zaleska, A. Doped-TiO_2: A Review. *Recent Patents Eng.* **2008**, *2*, 157–164. [CrossRef]
7. Sescu, A.M.; Favier, L.; Lutic, D.; Soto-Donoso, N.; Ciobanu, G.; Harja, M. TiO_2 Doped with Noble Metals as an Efficient Solution for the Photodegradation of Hazardous Organic Water Pollutants at Ambient Conditions. *Water* **2021**, *13*, 19. [CrossRef]
8. Hsini, A.; Naciri, Y.; Laabd, M.; Bouziani, A.; Navío, J.; Puga, F.; Boukherroub, R.; Lakhmiri, R.; Albourine, A. Development of a novel PANI@WO3 hybrid composite and its application as a promising adsorbent for Cr(VI) ions removal. *J. Environ. Chem. Eng.* **2021**, *9*, 105885. [CrossRef]
9. Briffa, J.; Sinagra, E.; Blundell, R. Heavy metal pollution in the environment and their toxicological effects on humans. *Heliyon* **2020**, *6*, e04691. [CrossRef]
10. Laabd, M.; Imgharn, A.; Hsini, A.; Naciri, Y.; Mobarak, M.; Szunerits, S.; Boukherroub, R.; Albourine, A. Efficient detoxification of Cr(VI)-containing effluents by sequential adsorption and reduction using a novel cysteine-doped PANi@faujasite composite: Experimental study supported by advanced statistical physics prediction. *J. Hazard. Mater.* **2022**, *422*, 126857. [CrossRef]
11. Raguram, T.; Rajni, K.S. Synthesis and analysing the structural, optical, morphological, photocatalytic and magnetic properties of TiO_2 and doped (Ni and Cu) TiO_2 nanoparticles by sol–gel technique. *Appl. Phys. A* **2019**, *125*, 288. [CrossRef]

12. Yadav, H.M.; Otari, S.; Koli, V.B.; Mali, S.S.; Hong, C.K.; Pawar, S.H.; Delekar, S.D. Preparation and characterization of copper-doped anatase TiO_2 nanoparticles with visible light photocatalytic antibacterial activity. *J. Photochem. Photobiol. A Chem.* **2014**, *280*, 32–38. [CrossRef]

13. Zhang, R.; Shao, M.; Xu, S.; Ning, F.; Zhou, L.; Wei, M. Photo-assisted synthesis of zinc-iron layered double hydroxides/TiO_2 nanoarrays toward highly-efficient photoelectrochemical water splitting. *Nano Energy* **2017**, *33*, 21–28. [CrossRef]

14. Bashiri, R.; Norani, M.M.; Kait, C.F.; Sufian, S. Study on Synthesis and Characterization of Cu-Ni Doped TiO_2 by Sol-Gel Hydrothermal. *Adv. Mater. Res.* **2014**, *925*, 248–252. [CrossRef]

15. Liu, B.; Chen, H.M.; Liu, C.; Andrews, S.C.; Hahn, C.; Yang, P. Large-Scale Synthesis of Transition-Metal-Doped TiO_2 Nanowires with Controllable Overpotential. *J. Am. Chem. Soc.* **2013**, *135*, 9995–9998. [CrossRef]

16. Shakil, R.; El-Sawy, A.M.; Tasnim, H.; Meguerdichian, A.G.; Jin, J.; Dubrosky, J.P.; Suib, S.L. Single-Doped and Multidoped Transition-Metal (Mn, Fe, Co, and Ni) ZnO and Their Electrocatalytic Activities for Oxygen Reduction Reaction. *Inorg. Chem.* **2018**, *57*, 9977–9987. [CrossRef]

17. Yadav, S.; Jaiswar, G. Review on Undoped/Doped TiO_2 Nanomaterial; Synthesis and Photocatalytic and Antimicrobial Activity. *J. Chin. Chem. Soc.* **2017**, *64*, 103–116. [CrossRef]

18. Naciri, Y.; Hsini, A.; Bouziani, A.; Tanji, K.; El Ibrahimi, B.; Ghazzal, M.; Bakiz, B.; Albourine, A.; Benlhachemi, A.; Navío, J.; et al. Z-scheme WO3/PANI heterojunctions with enhanced photocatalytic activity under visible light: A depth experimental and DFT studies. *Chemosphere* **2022**, *292*, 133468. [CrossRef]

19. Imgharn, A.; Anchoum, L.; Hsini, A.; Naciri, Y.; Laabd, M.; Mobarak, M.; Aarab, N.; Bouziani, A.; Szunerits, S.; Boukherroub, R.; et al. Effectiveness of a novel polyaniline@Fe-ZSM-5 hybrid composite for Orange G dye removal from aqueous media: Experimental study and advanced statistical physics insights. *Chemosphere* **2022**, *295*, 133786. [CrossRef]

20. Imgharn, A.; Ighnih, H.; Hsini, A.; Naciri, Y.; Laabd, M.; Kabli, H.; Elamine, M.; Lakhmiri, R.; Souhail, B.; Albourine, A. Synthesis and characterization of polyaniline-based biocomposites and their application for effective removal of Orange G dye using adsorption in dynamic regime. *Chem. Phys. Lett.* **2021**, *778*, 138811. [CrossRef]

21. Fahoul, Y.; Tanji, K.; Zouheir, M.; El Mrabet, I.; Naciri, Y.; Hsini, A.; Nahali, L.; Kherbeche, A. Novel River Sediment@ZnO Co nanocomposite for photocatalytic degradation and COD reduction of crystal violet under visible light. *J. Mol. Struct.* **2022**, *1253*, 132298. [CrossRef]

22. Mimouni, I.; Bouziani, A.; Naciri, Y.; Boujnah, M.; El Belghiti, M.A.; El Azzouzi, M. Effect of heat treatment on the photocatalytic activity of α-Fe_2O_3 nanoparticles: Towards diclofenac elimination. *Environ. Sci. Pollut. Res.* **2021**, *29*, 7984–7996. [CrossRef] [PubMed]

23. Aguilar, T.; Navas, J.; Alcántara, R.; Lorenzo, C.F.; Gallardo, J.; Blanco, G.; Martín-Calleja, J. A route for the synthesis of Cu-doped TiO_2 nanoparticles with a very low band gap. *Chem. Phys. Lett.* **2013**, *571*, 49–53. [CrossRef]

24. Mogal, S.I.; Mishra, M.; Gandhi, V.G.; Tayade, R.J. Metal Doped Titanium Dioxide: Synthesis and Effect of Metal Ions on Physico-Chemical and Photocatalytic Properties. *Mater. Sci. Forum* **2013**, *734*, 364–378. [CrossRef]

25. Hampel, B.; Pap, Z.; Sapi, A.; Szamosvolgyi, A.; Baia, L.; Hernadi, K. Application of TiO_2-Cu Composites in Photocatalytic Degradation Different Pollutants and Hydrogen Production. *Catalysts* **2020**, *10*, 85. [CrossRef]

26. Zhang, J.; Zhou, P.; Liu, J.; Yu, J. New understanding of the difference of photocatalytic activity among anatase, rutile and brookite TiO_2. *Phys. Chem. Chem. Phys.* **2014**, *16*, 20382–20386. [CrossRef]

27. Scanlon, D.O.; Dunnill, C.W.; Buckeridge, J.; Shevlin, S.A.; Logsdail, A.J.; Woodley, S.M.; Catlow, C.R.A.; Powell, M.J.; Palgrave, R.G.; Parkin, I.P.; et al. Band alignment of rutile and anatase TiO_2. *Nat. Mater.* **2013**, *12*, 798–801. [CrossRef]

28. Luttrell, T.; Halpegamage, S.; Tao, J.; Kramer, A.; Sutter, E.; Batzill, M. Why is anatase a better photocatalyst than rutile?—Model studies on epitaxial TiO_2 films. *Sci. Rep.* **2014**, *4*, 4043. [CrossRef]

29. Zhang, D.; Zeng, F. Photocatalytic oxidation of organic dyes with visible-light-driven codoped TiO_2 photocatalysts. *Russ. J. Phys. Chem. A* **2011**, *85*, 1077–1083. [CrossRef]

30. Tobaldi, D.; Piccirillo, C.; Rozman, N.; Pullar, R.; Seabra, M.; Škapin, A.S.; Castro, P.; Labrincha, J. Effects of Cu, Zn and Cu-Zn addition on the microstructure and antibacterial and photocatalytic functional properties of Cu-Zn modified TiO_2 nano-heterostructures. *J. Photochem. Photobiol. A Chem.* **2016**, *330*, 44–54. [CrossRef]

31. Khairy, M.; Zakaria, W. Effect of metal-doping of TiO_2 nanoparticles on their photocatalytic activities toward removal of organic dyes. *Egypt. J. Pet.* **2014**, *23*, 419–426. [CrossRef]

32. Niu, B.; Wang, X.; Wu, K.; He, X.; Zhang, R. Mesoporous Titanium Dioxide: Synthesis and Applications in Photocatalysis, Energy and Biology. *Materials* **2018**, *11*, 1910. [CrossRef]

33. Hernández, S.; Hidalgo, D.; Sacco, A.; Chiodoni, A.; Lamberti, A.; Cauda, V.; Tresso, E.; Saracco, G. Comparison of photocatalytic and transport properties of TiO_2 and ZnO nanostructures for solar-driven water splitting. *Phys. Chem. Chem. Phys.* **2015**, *17*, 7775–7786. [CrossRef] [PubMed]

34. Reddam, H.A.; Elmail, R.; Lloria, S.C.; Tomás, G.M.; Reddam, Z.A.; Coloma-Pascual, F. Synthesis of Fe, Mn and Cu modified TiO_2 photocatalysts for photodegradation of Orange II. *Boletín de la Sociedad Española de Cerámica y Vidrio* **2020**, *59*, 138–148. [CrossRef]

35. Mishra, A.P.; Sharma, N.; Jain, R.K. Microwave Synthesis, Spectral, Thermal and Antimicrobial Studies of Some Ni(II) and Cu(II) Schiff Base Complexes. *Open J. Synth. Theory Appl.* **2012**, *2*, 56–62. [CrossRef]

36. Arévalo-Pérez, J.C.; De La Cruz-Romero, D.; García, A.C.; Lobato-García, C.E.; Aguilar-Elguezabal, A.; Torres-Torres, J.G. Photodegradation of 17 α-methyltestosterone using TiO_2-Gd^{3+} and TiO_2-Sm^{3+} photocatalysts and simulated solar radiation as an activation source. *Chemosphere* **2020**, *249*, 126497. [CrossRef] [PubMed]

37. Cordero-García, A.; Palomino, G.T.; Hinojosa-Reyes, L.; Guzmán-Mar, J.L.; Maya-Teviño, L.; Hernández-Ramírez, A. Photocatalytic behaviour of WO_3/TiO_2-N for diclofenac degradation using simulated solar radiation as an activation source. *Environ. Sci. Pollut. Res.* **2016**, *24*, 4613–4624. [CrossRef]

38. Cordero-García, A.; Guzmán-Mar, J.; Hinojosa-Reyes, L.; Ruiz-Ruiz, E.; Hernández-Ramírez, A. Effect of carbon doping on WO_3/TiO_2 coupled oxide and its photocatalytic activity on diclofenac degradation. *Ceram. Int.* **2016**, *42*, 9796–9803. [CrossRef]

39. Mathew, S.; Ganguly, P.; Rhatigan, S.; Kumaravel, V.; Byrne, C.; Hinder, S.J.; Bartlett, J.; Nolan, M.; Pillai, S.C. Cu-Doped TiO_2: Visible Light Assisted Photocatalytic Antimicrobial Activity. *Appl. Sci.* **2018**, *8*, 2067. [CrossRef]

40. Obregón, S.; Muñoz-Batista, M.J.; Fernández-García, M.; Kubacka, A.; Colón, G. Cu–TiO_2 systems for the photocatalytic H_2 production: Influence of structural and surface support features. *Appl. Catal. B: Environ.* **2015**, *179*, 468–478. [CrossRef]

41. Xu, D.; Fan, D.; Shen, W. Catalyst-free direct vapor-phase growth of Zn1−xCuxO micro-cross structures and their optical properties. *Nanoscale Res. Lett.* **2013**, *8*, 46. [CrossRef] [PubMed]

42. Wang, M.; Jiang, L.; Kim, E.J.; Hahn, S.H. Electronic structure and optical properties of $Zn(OH)_2$: LDA+U calculations and intense yellow luminescence. *RSC Adv.* **2015**, *5*, 87496–87503. [CrossRef]

43. Thirupathi, B.; Smirniotis, P.G. Co-doping a metal (Cr, Fe, Co, Ni, Cu, Zn, Ce, and Zr) on Mn/TiO_2 catalyst and its effect on the selective reduction of NO with NH3 at low-temperatures. *Appl. Catal. B: Environ.* **2011**, *110*, 195–206. [CrossRef]

44. Adrover, E.; Boldrini, D.; Divins, N.J.; Casanovas, A.; Tonetto, G.; López, E.; Llorca, J. Study of Cu-Zn and Au/TiO2 catalysts on anodized aluminum monoliths for hydrogen generation and purification. *Int. J. Chem. React. Eng.* **2016**, *14*, 831–842. [CrossRef]

45. Mizutani, U. Hume-Rothery rules for structurally complex alloy phases. *MRS Bull.* **2012**, *37*, 169. [CrossRef]

46. Sulaiman, S.N.A.; Noh, M.Z.; Adnan, N.N.; Bidin, N.; Ab Razak, S.N. Ab Razak, Effects of photocatalytic activity of metal and non-metal doped TiO_2 for Hydrogen production enhancement—A Review. *J. Phys. Conf. Ser.* **2018**, *5*, 1027–1045. [CrossRef]

47. Rana, A.G.; Ahmad, W.; Al-Matar, A.; Shawabkeh, R.; Aslam, Z. Synthesis and characterization of Cu–Zn/TiO_2 for the photocatalytic conversion of CO_2 to methane. *Environ. Technol.* **2017**, *38*, 1085–1092. [CrossRef]

48. Paulino, P.; Salim, V.M.; Resende, N. Zn-Cu promoted TiO_2 photocatalyst for CO_2 reduction with H_2O under UV light. *Appl. Catal. B Environ.* **2016**, *185*, 362–370. [CrossRef]